

Fuzzy Dynamic Sequential Predictive Control of Outer Rotor Coreless Bearingless Permanent Magnet Synchronous Generator Based on Prediction Error Compensation

Shuai Zhuang¹, Gai Liu^{2,*}, and Huangqiu Zhu^{1,*}

¹School of Electrical and Information Engineering, Jiangsu University, Zhenjiang 212013, China

²School of Electrical and Control Engineering, Xuzhou University of Technology, Xuzhou 221018, China

ABSTRACT: Outer rotor coreless bearingless permanent magnet synchronous generator is a complex and strongly coupled nonlinear system. The stable suspension and voltage of generator are always the focus and difficulty of research. The fuzzy dynamic sequential model predictive torque control method based on prediction error compensation is proposed. Firstly, the basic structure and working principle of the outer rotor coreless bearingless permanent magnet synchronous generator are introduced in this paper, and the mathematical model of voltage and suspension force is established. Secondly, the mathematical model is carried out to obtain the prediction equation, and the prediction error compensation is carried out to the prediction equation, and then the number of the first output voltage vectors is determined by fuzzy controller. Finally, the designed control system is simulated and experimentally studied. The simulated and experimental results show that this control method can obtain good voltage and suspension response, and the outer rotor coreless bearingless permanent magnet synchronous generator has good dynamic performance and stability.

1. INTRODUCTION

The traditional permanent magnet synchronous generator (PMSG) supports rotating shaft by mechanical bearings, which will cause serious friction and wear with the increase of rotating speed. Bearingless permanent magnet synchronous generator (BPMSG), a new kind of generator that combines magnetic bearing and permanent magnet synchronous generator, has features like a compact structure, light weight, high output power, etc. Further, in order to increase the rotational inertia of the generator and reduce the core loss, an outer rotor coreless bearingless permanent magnet synchronous generator (ORC-BPMSG) is proposed in this paper. Compared with the traditional PMSG, ORC-BPMSG has the advantages of no friction and wear, high efficiency, compact structure, no cogging torque, no core loss, and large rotational inertia, so ORC-BPMSG has a broad application prospect in wind turbines and flywheel energy storage systems [1–4]. In the field of motor control, there are two common control methods, vector control and direct torque control. The stator current is decomposed into d - and q -axes by vector control. The two components are controlled respectively, and then the motor flux and torque are controlled respectively. It has a good control accuracy, but there are complex coordinate transformations, and the system characteristics are greatly affected by the motor parameters. Direct torque control uses voltage vectors to directly control the torque and flux linkage of the motor. Without complex coordinate transformation, the structure is simpler, and good dynamic

performance can be obtained, but it is easy to produce large torque ripple and poor steady-state performance.

In recent years, with the development of microprocessor and power electronics technology, finite control set model predictive control (FCS-MPC), as a kind of closed-loop control algorithm using online optimization, can significantly improve the dynamic performance of motor and has been successfully applied in the field of motor drive [5]. Different from the control variables of the stator current d - and q -axis components of the same dimension in the model predicted current control (MPCC), the control variables of the model predicted torque control (MPTC) are flux and torque of different dimensions and orders of magnitude. It is necessary to set a weighting factor to balance the flux and torque, and the value of the weighting factor is dynamically adjusted with the motor state. In general, the adjustment of the weighting factors is mostly determined by experimental method, which is a tedious process [6].

To eliminate or reduce the weighting factors in MPTC, various methods have been proposed. In the literature [7, 8], they attempt to use algorithms to simplify the selection of weighting factors and modify the cost function of PTC. VlseKriterijuska Optimizacija I Komoromisno Resenje (VIKOR) and Technique for Order of Preference by Similarity to Ideal Solution (TOPSIS) methods are used in the cost function to eliminate the weighting factor, but the realization process is complicated. Ref. [9] constructs a torque error equation with the weight coefficient and designs the weighting factor with minimum torque error, but it is difficult to realize the design of fuzzy control rules. In [10], fuzzy logic control technique is used to dynam-

* Corresponding authors: Gai Liu (lg_just@163.com); Huangqiu Zhu (zhuhuangqiu@ujs.edu.cn).

ically adjust the weighting factors, and the optimal switching states are selected without retuning the weighting factors, but the design of fuzzy control rules is difficult to realize. In [11], artificial neural network algorithm (ANN) is used to achieve the automated selection of weighting factors, but there are also problems such as the need to construct a large number of training data sets, and the calculation of the algorithm is large. In [12, 13], the control variable is transformed into a dimensionless cost function ranking position, thus eliminating the weighting factors, but the cost function optimization is transformed into cost function ranking, which increases the amount of calculation and affects the real-time performance.

Sequential model predictive control (SMPC) is proposed in the literature [14], which can realize the predictive torque and flux control of motor without using weighting factors, eliminating the use of weighting factors in MPC. This method first evaluates the torque and selects two smaller voltage vectors according to the cost function of torque. These two voltage vectors are then sent to the second cost function of flux, thus selecting the optimal voltage vector. This method is slightly simple and solves the problem of difficult calculation with weighting factors. However, the first stage evaluates the torque first, and only two voltage vectors are selected, so the priority of the torque is higher. Ref. [15] improves on [14] and proposes a generalized sequential model predictive control (GSMPC). Ref. [14] can only refer to torque as the first stage and flux as the second stage. If the sequence is switched, the control system may not work. In this regard, [15] changes the number of voltage vectors selected by the first level cost function to three, so that a better balance between torque and flux can be achieved. After the change, the torque and flux can work effectively regardless of who is predicting it as the first stage. Although the GSMPC has better stability, its computational load is greatly increased.

Based on this, a fuzzy dynamic sequential model predictive torque control (FD-SMPTC) based on prediction error compensation of the ORC-BPMSG is proposed in this paper. The improved FD-SMPTC is proposed by slightly modifying the previous SMPTC. Compared with the traditional SMPTC, the proposed FD-SMPTC still adopts the sequential control structure of the torque control and flux control, which selects the optimal voltage vector by sequentially evaluating two separate cost functions. However, different from the traditional SPMC, FD-SMPTC uses a fuzzy controller to dynamically adjust the number of output voltage vectors according to the running state of the motor to optimize the control performance of the system. Compared with GSMPC, unnecessary computation is reduced. Furthermore, as the torque prediction process depends on a large number of motor parameters, which will change under the influence of external factors such as temperature rise and magnetic field saturation, there will be an error in the torque prediction results, which will further affect the selection of output vectors of the FD-SMPTC, resulting in tracking error in the output torque of the system. Therefore, a prediction error compensation based on proportional integral (PI) is designed to eliminate the influence of parameter change on the torque prediction, so that the control method has strong robustness.

Finally, the effectiveness and reliability of the method are verified by simulation and experiments.

2. OPERATION PRINCIPLE AND MATHEMATICAL OF THE ORC-BPMSG

2.1. Operation Principle of ORC-BPMSG

Compared with the traditional PMSG, ORC-BPMSG has two sets of windings in the stator, which are power generation windings and suspension force windings. If the pole-pair of the suspension force windings P_2 and the pole-pair number of the power generation windings P_1 meet the relationship of $P_1 = P_2 \pm 1$, and the rotation direction and electric angular velocity of the magnetic field generated by the suspension force windings and the power generation windings are consistent, the conditions for realizing the suspension of the motor rotor are met. ORC-BPMSG works the same way as regular PMSG. The power generation windings are rotated by the prime mover to cut the magnetic inductance lines and generate a voltage in the power generation windings.

As shown in Fig. 1, there are two sets of windings in the stator. The outer layer is a power generation windings with pole-pair number P_1 of 3. The inner layer is a suspension force windings with pole-pair number P_2 of 2. The power generation windings are responsible for generating electromagnetic torque to realize the rotation of the rotor. The suspension force windings control the radial suspension force to realize the stable suspension of the rotor.

When the current as shown in Fig. 1 is passed into suspension force windings, the magnetic field at air gap 1 increases; the magnetic field at air gap 2 weakens; and air gaps 3 and 4 are still in balance, so the radial suspension force F_x along the direction of magnetic field enhancement will be generated in the rotor. Similarly, by adjusting the current passing through the suspension force windings, a variable suspension force F_y along the y axis can be generated on the rotor. To sum up, by controlling the phase and amplitude of the current passing through the suspension force windings, the radial suspension force of any size and direction can be generated on the rotor, and the rotor can be stably suspended on the radial two degrees of freedom.

2.2. Mathematical Model of ORC-BPMSG

The mathematical model of bearingless permanent magnet synchronous generator includes generation part mathematical model and suspension part mathematical model.

The mathematical model of the power generation voltage equation under the α - and β -axes can be written as:

$$\begin{cases} u_{1\alpha} = R_1 i_{1\alpha} + \frac{d\psi_{1\alpha}}{dt} \\ u_{1\beta} = R_1 i_{1\beta} + \frac{d\psi_{1\beta}}{dt} \end{cases} \quad (1)$$

$$\begin{cases} \psi_{1\alpha} = L_s i_{1\alpha} - \psi_f \sin \theta \\ \psi_{1\beta} = L_s i_{1\beta} + \psi_f \cos \theta \end{cases} \quad (2)$$

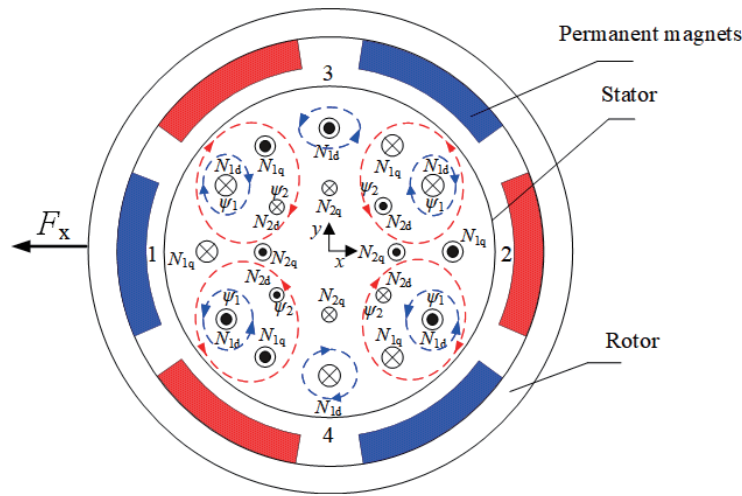


FIGURE 1. Principle of suspension force generation.

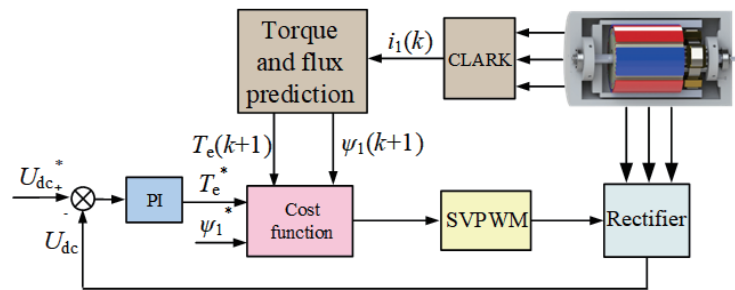


FIGURE 2. Traditional model predictive torque control block diagram.

where $u_{1\alpha}$ and $u_{1\beta}$ are voltage components of the α - and β -axes of the power generation windings; $i_{1\alpha}$ and $i_{1\beta}$ are the current components of the α - and β -axes of the power generation windings; $\psi_{1\alpha}$ and $\psi_{1\beta}$ are the magnetic linkage components of the α - and β -axes of the power generation windings; R_1 is the resistance value of the power generation windings; L_s is the inductance of the power generation windings.

The torque equation is:

$$T_e = \frac{3}{2} P_1 (\psi_{1\alpha} i_{1\beta} - \psi_{1\beta} i_{1\alpha}) \quad (3)$$

where P_1 is the number of pole-pairs of the power generation windings.

According to Maxwell's tensor method, the expression of the suspension force of the ORC-BPMSG in the α - and β -axes can be simplified as:

$$\begin{cases} F_\alpha = \frac{\pi P_1 P_2}{8lr\mu_0 N_1 N_2} \psi_m \psi_2 \cos(\lambda - \mu_2) \\ F_\beta = \frac{\pi P_1 P_2}{8lr\mu_0 N_1 N_2} \psi_m \psi_2 \sin(\lambda - \mu_2) \end{cases} \quad (4)$$

where ψ_2 is the suspension force windings flux linkage; μ_2 is the phase angle of the suspension force windings flux linkage ψ_2 ; λ is the phase angle of the air gap flux linkage ψ_m ; P_2 is

the number of pole-pairs of the suspension force windings; l is the length of the motor core; r is the motor rotor radius; N_1 and N_2 are the turns of power generation windings and suspension force windings; μ_0 is the vacuum permeability.

3. DYNAMIC SEQUENTIAL MODEL PREDICTIVE TORQUE CONTROL BASED ON PREDICTION ERROR COMPENSATION

3.1. Basic Thought

The traditional model predictive torque control is shown in Fig. 2.

The algorithm uses a value function to evaluate the control effect of six effective vectors and zero vector on torque and flux linkage. The commonly used tracking value function is defined as:

$$g = [T_e^* - T_e(k+1)]^2 + \lambda [\psi_1^* - \psi_1(k+1)]^2 \quad (5)$$

3.2. Power Generation Prediction Model

Firstly, the current prediction model is constructed. In the α - and β -axes, applying the first-order Euler's formula to discretize the mathematical model of power generation windings, the stator current prediction equations at the $k+1$ moment are

as follows:

$$\begin{cases} i_{1\alpha}(k+1) = i_{1\alpha}(k) + (u_{1\alpha}(k) - R_1 i_{1\alpha}(k) - j\omega\psi_f e^{j\theta})T_s/L_s \\ i_{1\beta}(k+1) = i_{1\beta}(k) + (u_{1\beta}(k) - R_1 i_{1\beta}(k) - j\omega\psi_f e^{j\theta})T_s/L_s \end{cases} \quad (6)$$

where $i_{1\alpha}(k+1)$ and $i_{1\beta}(k+1)$ are the components of stator current in the α - and β -axes at the $k+1$ moment.

According to the flux and torque prediction algorithm, the expressions of flux and torque are respectively obtained:

$$\begin{cases} \psi_{1\alpha}(k+1) = \psi_{1\alpha}(k) + [u_{1\alpha}(k) - R_1 i_{1\alpha}(k)]T_s \\ \psi_{1\beta}(k+1) = \psi_{1\beta}(k) + [u_{1\beta}(k) - R_1 i_{1\beta}(k)]T_s \\ \psi_1(k+1) = \sqrt{\psi_{1\alpha}^2(k+1) + \psi_{1\beta}^2(k+1)} \end{cases} \quad (7)$$

$$T_e(k+1) = \frac{3}{2}P_1 \begin{pmatrix} \psi_{1\alpha}(k+1)i_{1\beta}(k+1) \\ -\psi_{1\beta}(k+1)i_{1\alpha}(k+1) \end{pmatrix} \quad (8)$$

where $\psi_{1\alpha}(k+1)$ and $\psi_{1\beta}(k+1)$ are the components of stator flux in the α - and β -axes of power generation windings at the $k+1$ moment.

3.3. Suspension Prediction Model

The ORC-BPMSG prediction direct suspension force control is based on direct suspension force control by using the prediction algorithm to achieve the goal of optimizing suspension force control. Rewrite (4) into matrix form and then carry out trigonometric transformation:

$$\begin{pmatrix} F_\alpha \\ F_\beta \end{pmatrix} = \frac{\pi P_1 P_2}{8lr\mu_0 N_1 N_2} \psi_m \begin{pmatrix} \cos \lambda & \sin \lambda \\ \sin \lambda & -\cos \lambda \end{pmatrix} \begin{pmatrix} \psi_{2\alpha} \\ \psi_{2\beta} \end{pmatrix} \quad (9)$$

According to Equation (9), the suspension force depends on the air gap flux ψ_m of the power generation windings and the suspension force windings flux ψ_2 . In order to obtain the predicted value of the suspension force, $\psi_m(k+1)$ and $\psi_2(k+1)$ should be obtained respectively. Similar to equation (7), the suspension force windings flux $\psi_2(k+1)$ at $k+1$ moment can be obtained by discrete algorithm after real-time observation by flux observer:

$$\begin{cases} \psi_{2\alpha}(k+1) = \psi_{2\alpha}(k) + [u_{2\alpha}(k) - R_2 i_{2\alpha}(k)]T_s \\ \psi_{2\beta}(k+1) = \psi_{2\beta}(k) + [u_{2\beta}(k) - R_2 i_{2\beta}(k)]T_s \end{cases} \quad (10)$$

where $i_{2\alpha}$ and $i_{2\beta}$ are the current components of the α - and β -axes of the suspension force windings; $\psi_{2\alpha}$ and $\psi_{2\beta}$ are the magnetic linkage components of the α - and β -axes of the suspension force windings; R_2 is the resistance value of the suspension force windings.

The air gap flux of power generation windings is a composite flux of power generation windings flux and rotor permanent magnet flux. In the process of motor operation, considering the influence of windings leakage inductance, the air gap flux $\psi_m(k+1)$ of power generation windings at $k+1$ moment is:

$$\begin{cases} \psi_{m\alpha}(k+1) = \psi_{1\alpha}(k+1) - L_{1\delta} i_{1\alpha}(k+1) \\ \psi_{m\beta}(k+1) = \psi_{1\beta}(k+1) - L_{1\delta} i_{1\beta}(k+1) \end{cases} \quad (11)$$

where $L_{1\delta}$ is the leakage sense of power generation windings.

According to Equations (4), (7), and (11), the prediction expression of suspension force can be obtained:

$$\begin{cases} F_\alpha(k+1) = k_m \psi_{m\alpha}(k+1) \psi_2(k+1) \cos(\lambda - \mu_2) \\ F_\beta(k+1) = k_m \psi_{m\beta}(k+1) \psi_2(k+1) \sin(\lambda - \mu_2) \end{cases} \quad (12)$$

In order to realize the direct control of the suspension force, the suspension force can be taken as the optimization object directly. The expression g_3 of the cost function is expressed as [16]:

$$g_3 = [F_\alpha^* - F_\alpha(k+1)]^2 + [F_\beta^* - F_\beta(k+1)]^2 \quad (13)$$

3.4. Fuzzy Dynamic Sequential Model Predictive Torque Control

The traditional predictive torque control model contains weighting factor in the cost function, and there is no uniform criterion for the design of weighting factor, so the debugging process is complicated. The emergence of SMPC solves the above problems and simplifies the controller design.

The sequential model proposed in [14] predicts the use of a sequential structure to control multiple control objectives. Firstly, the torque of each voltage vector is calculated according to the cost function g_1 , and the two voltage vectors that are better are selected, and then sent to the second cost function g_2 for the flux comparison. The voltage vector that generates the least flux is selected as the final optimal voltage vector. This control strategy is simple and solves the difficult problem of the weighting factors design.

$$g_1 = [T_e^* - T_e(k+1)]^2 \quad (14)$$

$$g_2 = [\psi_1^* - \psi_1(k+1)]^2 \quad (15)$$

However, in the first cost function evaluation results, only two vectors are selected. And more emphasis is placed on torque performance. If the evaluation sequence is switched, the system can no longer operate stably at full speed. In this regard, [15] proposes a generalized SMPC, in which the order of cost functions 1 and 2 is not required, and the number of vectors to be evaluated in the second cost function is increased from 2 to 3. Although the calculation amount is increased, the method achieves a better balance between torque and flux.

The running state of the motor is dynamically changing, and the importance of the control objective should also be dynamically changed to better meet the system requirements. The number of output voltage vectors of the first stage reflects the importance of the first level of control, but if the number of the first stage's output voltage vectors is too little or too much, it will cause the second level to lose control, so the number of the first stage's output voltage vectors is generally 2 or 3.

To sum up, this paper proposes a type of fuzzy cascaded model predictive control, which takes cost function 1 as the first level and cost function 2 as the second level. The number of output voltage vectors of the first stage is dynamically adjusted according to the state of the system. The following uses a fuzzy controller to adjust the number of output voltages

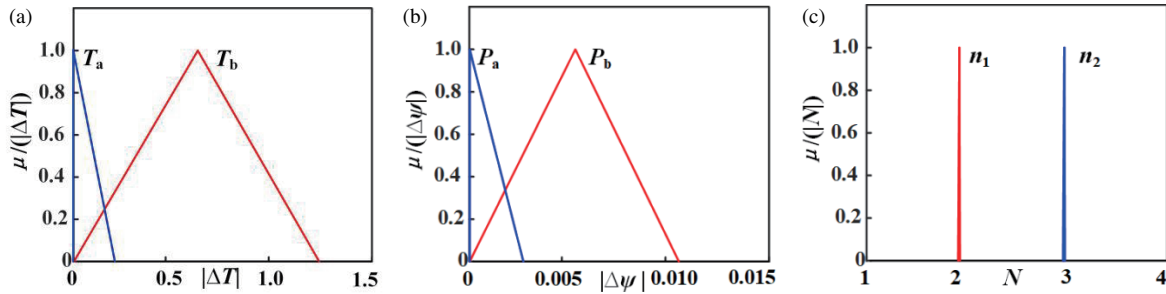


FIGURE 3. Degree of membership function. (a) Absolute torque error. (b) Absolute flux error. (c) N .

of the first stage to dynamically adjust the importance of different control objectives and optimize the control performance of the system.

The fuzzy controller uses the absolute value of motor torque error and flux error as input variables, and the number of first-stage output vectors N as output variables. The domain of absolute torque error $|\Delta T|$ is $[0 \text{ N}\cdot\text{m}, 1.5 \text{ N}\cdot\text{m}]$, which is divided into two fuzzy subsets $\{T_a, T_b\}$. The domain of absolute flux error $|\Delta\psi|$ is $[0 \text{ Wb}, 0.015 \text{ Wb}]$, which is divided into two fuzzy subsets $\{P_a, P_b\}$. The output domain of N is $[1, 4]$, divided into three fuzzy subsets $\{n_1, n_2\}$. The membership function is shown in Fig. 3.

The fuzzy control rules are shown in Table 1. After Mamdani fuzzy reasoning, the maximum membership degree average method is used to solve the fuzzy and output.

TABLE 1. Fuzzy control rule.

| N | $ \Delta T $ | | |
|----------------|--------------|-------|-------|
| | T_a | T_b | |
| $ \Delta\psi $ | P_a | n_2 | n_1 |
| | P_b | n_1 | n_1 |

The flowchart of the proposed FD-SMPC is shown in Fig. 4, and the operation process of FD-SMPC is briefly summarized as follows.

Layer 1: Extract current $i(k)$ and voltage s at moment k .

Layer 2: Apply the voltage vectors calculated in the previous sampling interval.

Layer 3: Estimate flux linkage and current at sampling interval k .

Layer 4: Calculate g_1 for all 7 voltage vectors.

Layer 5: Select the two or three vectors that make g_1 minimum based on the fuzzy reasoning above.

Layer 6: Compute g_2 of the two or three vectors selected in the previous step.

Layer 7: Select the voltage vector with the smallest g_2 applied in the next sampling interval.

3.5. Predictive Error Compensation

The above equations depend on the electrical resistance and inductance parameters of the motor. The inductance of the prototype used in this experiment is $L_{1d} = L_{1q} = 13.42 \text{ mH}$.

However, these parameters may not be precisely determined or change during the operation of the motor due to temperature increase or magnetic saturation. Therefore, the motor parameters used in these equations may not match their actual values. This results in inaccurate torque and flux predictions, which can affect the accuracy of model predictive control. These uncertainties can lead to inaccurate predictions of system behavior at a given voltage vector and reduce the robustness of the prediction algorithm. Fig. 5 shows the torque prediction error.

Considering the above explanation, the error compensation of the predicted torque value and the predicted flux value is made due to the parameter mismatch and other factors.

$$\begin{cases} T_e^P(k+1) = T_e(k+1) + \Delta T(k) \\ \psi_1^P(k+1) = \psi_1(k+1) + \Delta\psi(k) \end{cases} \quad (16)$$

where $T_e(k+1)$ and $\psi_1(k+1)$ are the predicted values of torque and stator flux amplitude at $k+1$ moment. $T_e^P(k+1)$ and $\psi_1^P(k+1)$ are the actual values of torque and stator flux amplitude at $k+1$ moment. $\Delta T(k)$ is the torque prediction error compensation; $\Delta\psi(k)$ is the flux prediction error compensation, but considering the small stator pressure drop, the influence of $\Delta\psi(k)$ on the flux amplitude can be ignored.

The cost function considering the prediction error compensation can be rewritten as:

$$g_1 = [T_e^* - T_e^P(k+1)]^2 \quad (17)$$

$$g_2 = [\psi_1^* - \psi_1^P(k+1)]^2 \quad (18)$$

Therefore, this paper constructs a prediction error compensation based on PI to enhance the robustness of the torque prediction model.

In Fig. 6, K_{pe} , K_{ie} , and K_{ce} are the ratio, integral and anti-integral saturation coefficients of the prediction error compensation respectively; $\Delta T(k)$ is the output of the moment k compensation to eliminate the interference of factors such as parameter mismatch on the torque prediction results and achieve the purpose of modifying the prediction model. In practical applications, the value of K_{pe} ranges from 0 to 1, and the value of K_{ie} should ensure that the dynamic time of the compensation is slightly longer than the torque adjustment time of the motor, so as to avoid torque oscillation in the transient state. The selection of parameters is based on the experience of traditional

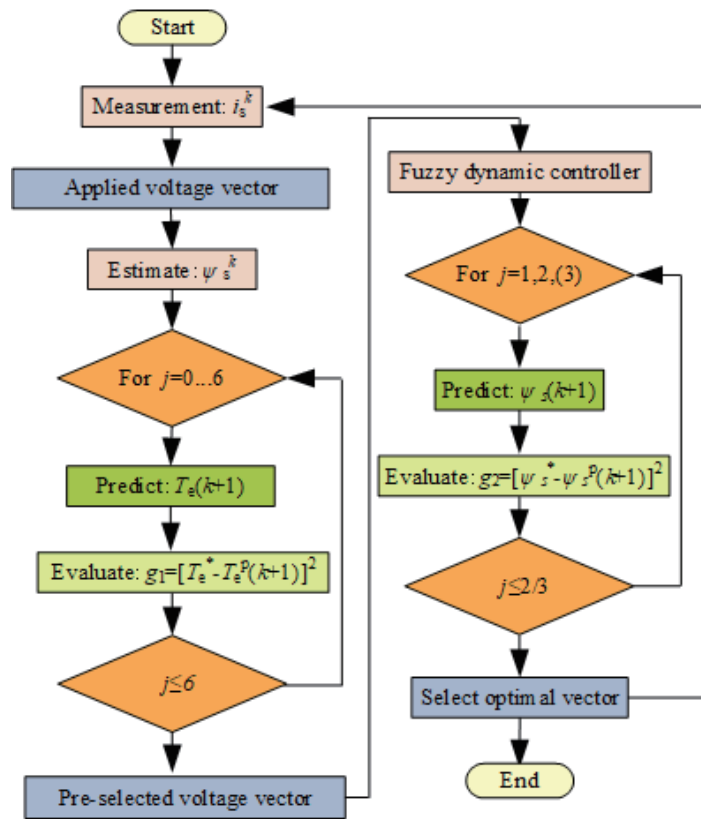


FIGURE 4. Flow diagram of the proposed FD-SMPTC.

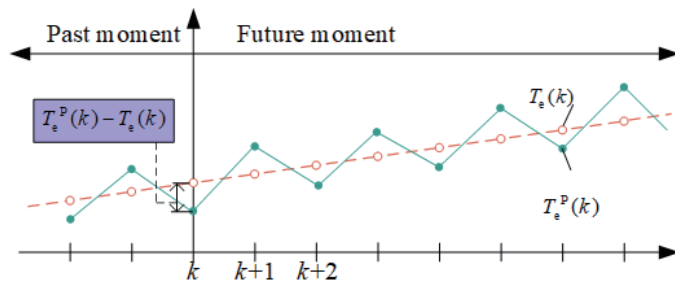


FIGURE 5. Torque prediction error.

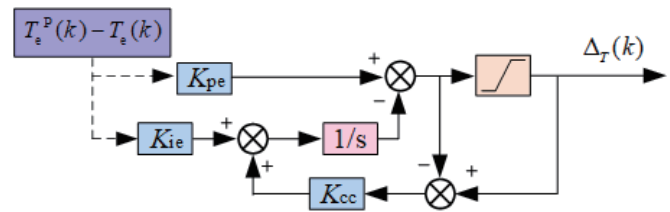


FIGURE 6. Prediction error compensation based on PI.

PI parameter design and the research of previous scholars, and then the appropriate adjustment is made according to the experimental data. In this experiment, $K_{pe} = 0.6$, $K_{ie} = 150$, $K_{cc} = 10$.

The control block diagram of the ORC-BPMSG based on FD-SMPTC is shown in Fig. 7.

4. SIMULATION TEST

According to the control block diagram shown in the Fig. 7, the proposed method is constructed and simulated by using Simulink toolbox in Matlab.

The simulation comparison of voltage characteristic curves is shown in Fig. 8. Traditional VC and the proposed FD-SMTPC are used for comparative analysis. It can be seen from Fig. 8 that the proposed FD-SMTPC reaches the stable generation volt-

age faster than the traditional VC control and has almost no overshoot, which is much smaller than 1.8% of the traditional VC. At 0.3 s, raising the given voltage to 250 V, FD-SMTPC is 0.028 s earlier than traditional VC. In addition, when the two methods are stabilized at 250 V, the voltage jitter amplitude is less than 9 V, that is, the ripple coefficient is less than 3.6%. The proposed FD-SMTPC has better tracking performance and dynamic response.

The radial displacement curves of the rotor in the x - and y -direction are shown in Fig. 9. Because the control system is a high-order system, there will be some overshoot when using traditional proportion integration differentiation (PID) control. It can be seen from Fig. 9(a) that in the process of motor acceleration, in the x direction, the maximum radial displacement value of traditional VC is 276 μm , and the stability time is 0.182 s, while the maximum radial displacement of direct

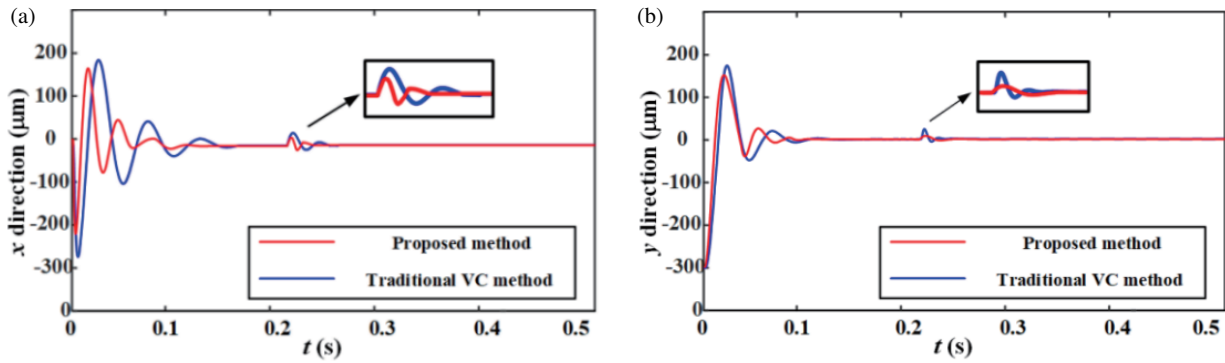


FIGURE 9. Simulation results at radial displacement of the rotor. (a) In the x direction. (b) In the y direction.

form of this paper is shown in Fig. 10, which mainly includes: the ORC-BPMSG prototype, digital signal processor (DSP), inverter, eddy current displacement sensor, oscilloscope, and PC host. In order to ensure the accuracy of the experimental comparison, all experimental environments and experimental settings are the same, and only the control methods are different.

The parameters of the prototype are shown in Table 2. TMS320F28335 is used as the controller to build the digital control system. The human-computer integrated interface is developed by VB6.0 software to realize on-line monitoring of experimental data and on-line adjustment of related control parameters.

TABLE 2. Main parameters of ORC-BPMSG.

| Parameters | Values |
|--|--------------|
| Rated power | 2 kW |
| Rated speed | 10 000 r/min |
| Rotor outer diameter | 200 mm |
| Rotor inner diameter | 180 mm |
| Air gap length | 2 mm |
| Permanent magnet thickness | 6 mm |
| Number of pole-pair of power generation windings | 3 |
| Number of polepair of suspension force windings | 2 |
| Polar arc coefficient | 0.78 |

The specific data of the ORC-BPMSG prototype is shown in Table 2.

The gain values of both PID and PI controllers are shown in Table 3.

TABLE 3. The gain values of both PID and PI controllers.

| Symbol | k_p | k_i | k_d |
|-----------------------------|-------|-------|-------|
| Voltage controller | 0.15 | 140 | |
| Displacement x controller | 3e7 | 7e7 | 2e3 |
| Displacement y controller | 3e5 | 6e7 | 2e3 |

5.1. Displacement of Rotor Center Experiment

Figure 11 shows the displacement diagram of the rotor center when the generation voltage is 100 V. It can be seen from Fig. 11 that using the proposed method results in a smaller displacement of the rotor, or it can be said that the rotor is more stable near the equilibrium point. The proposed control method improves the stability of rotor position balance. The proposed control reduces the maximum offset of the rotor center of mass by 37.5% compared to the use of traditional VC.

5.2. Voltage Regulation Experiment

Figure 12 shows the experiment results of different generation voltage. Fig. 12(a) and Fig. 12(b) are comparison diagrams of the generation voltage and corresponding in the x - and y -direction radial displacements using traditional VC and proposed method. In the voltage regulation experiment of 200 V to 250 V, Fig. 12(a) shows that the voltage regulation time of traditional VC is 114 ms, and there is an overshoot about 12 V. The radial displacements in the x - and y -directions are 39 μm and 52 μm , respectively. Fig. 12(b) shows that, when the proposed method is used, the voltage regulation time is 83 ms; the voltage response is 27.2% faster than the traditional VC; and there is almost no overshoot. The radial displacements in the x - and y -directions are 27 μm and 39 μm , respectively. Compared with the traditional VC, the radial displacement fluctuations in the x - and y -directions are reduced by 30.7% and 19.2%, respectively.

5.3. Dynamic Suspension Experiment

Figure 13 shows the radial displacement under the interference force of 10 N in the x direction when the generation voltage is stable at 250 V. The anti-interference displacement vibration experimental diagram controlled is also shown in Fig. 13. It can be seen from Fig. 13(a) that when traditional VC is used, the jitter amplitude in the x direction is 51 μm , and the jitter amplitude in the y direction is 38 μm . Then the 10 N disturbance is applied in the x direction; the maximum displacement deviation in the y direction is 53 μm ; and the adjustment time is 51 ms. When the proposed method is used, the jitter amplitude in the x direction is 32 μm , and the jitter amplitude in the y direction is 27 μm . The 10 N disturbance is applied in the

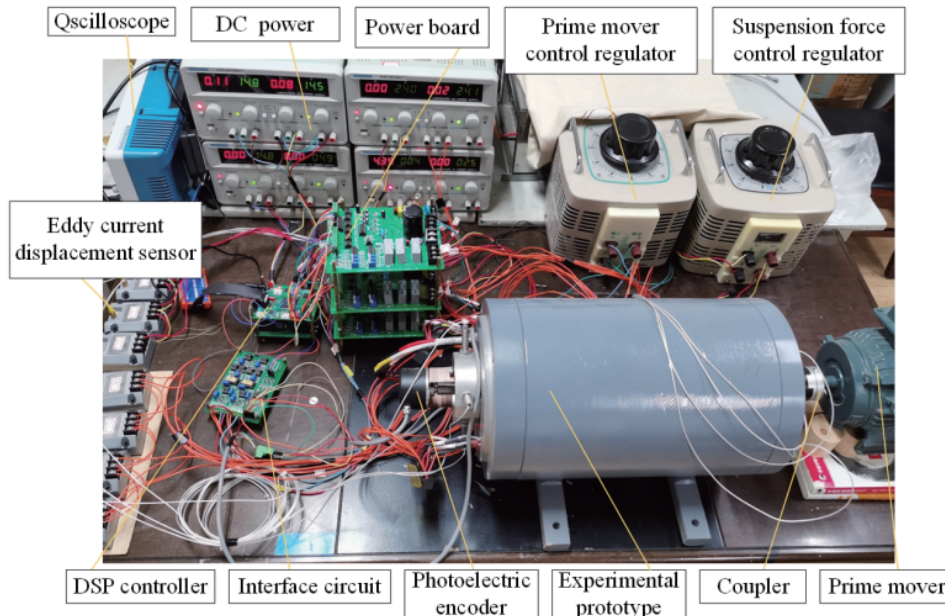


FIGURE 10. Experiment platform.

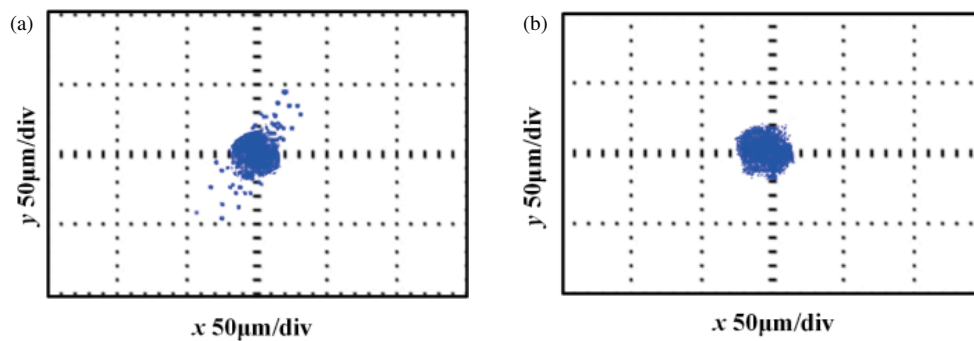


FIGURE 11. Experimental displacement of the rotor center. (a) Traditional VC. (b) Proposed method.

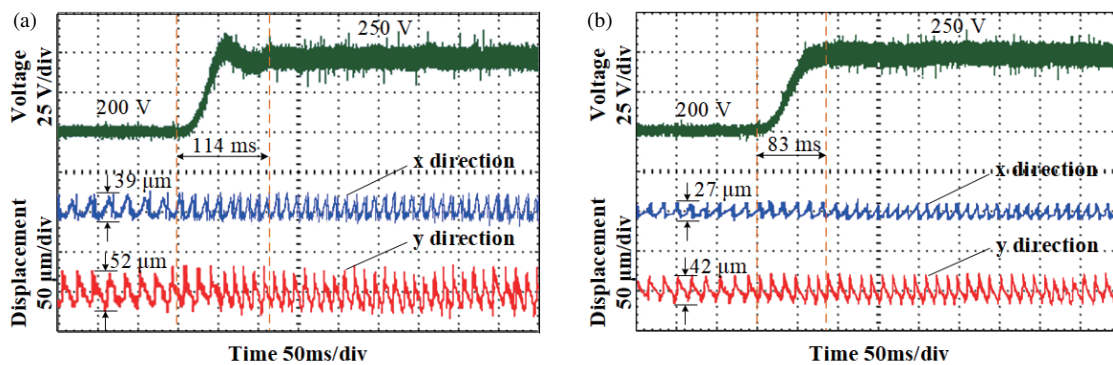


FIGURE 12. Experimental voltage regulation and corresponding in the x - and y -direction radial displacement. (a) Traditional VC. (b) Proposed method.

x direction; the maximum displacement deviation in the y direction is $41\ \mu\text{m}$; and the adjustment time is $45\ \text{ms}$. Compared with the traditional VC, the maximum displacement deviation is reduced by 22.6% , and the adjustment time is accelerated by 11.7% .

5.4. Parameter Robustness Experiment

Figure 14 shows the torque waveform of the motor when the generation voltage is $200\ \text{V}$. It can be seen from Fig. 14(a) that when the motor is at rated parameters, the traditional VC control torque ripple is larger. It can be seen from Fig. 14(b) that

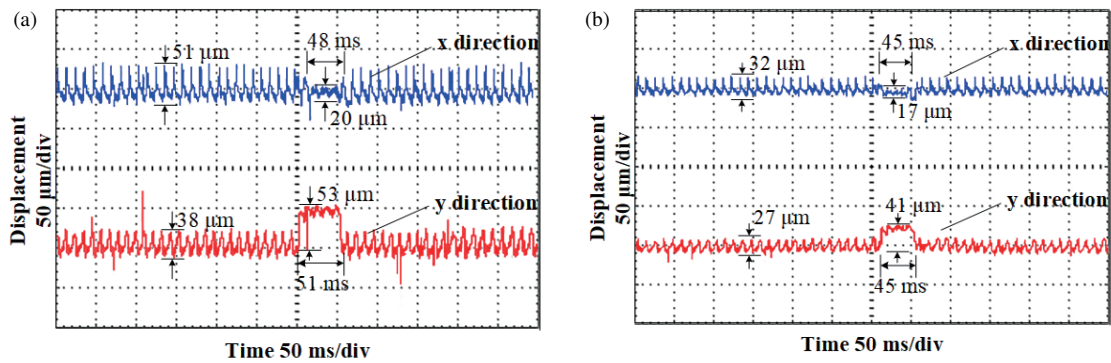


FIGURE 13. Influence of power generation voltage change on radial displacement. (a) Traditional VC. (b) Proposed method.

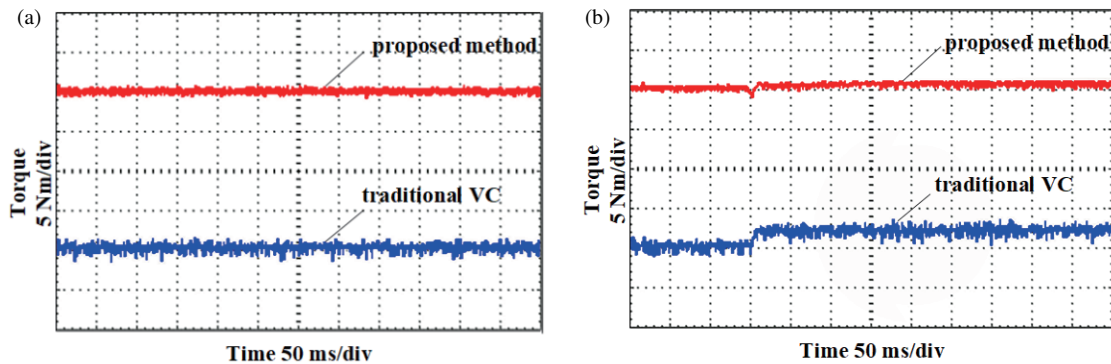


FIGURE 14. Torque waveform of the proposed method and the traditional VC. (a) Rated parameter. (b) Parameter mismatch.

when the motor parameter is changed to the 1.2 times rated parameter that is the parameter mismatch, the proposed method still has a good torque tracking. The traditional VC has a large deviation, and the torque ripple increases. Experimental results show that the proposed method has better static and dynamic performance than the traditional VC control method, improves the parameter robustness, and guarantees the control performance of the system.

6. CONCLUSION

In this paper, FD-SMPTC is applied to ORC-BPMSG, and the effectiveness of the controller is verified by simulation and experiments. The following conclusions are obtained:

1. The number of voltage vectors output at the first stage in the sequence structure has a great impact on the performance of the system, so it needs to be set reasonably. The optimal number of output voltage vectors can be selected dynamically by using a fuzzy controller according to the operating state of the voltage.
2. The numerical changes of stator resistance, inductance, and rotor flux will affect the torque prediction accuracy of the algorithm, resulting in tracking errors in system output torque. Therefore, a prediction error compensation based on PI is designed in the algorithm, and a robust torque prediction model is established to eliminate the influence of

parameter changes on torque prediction, so that the algorithm has strong parameter robustness.

3. The ORC-BPMSG digital control system is constructed, and the generation voltage response and suspension performance tests are carried out. Because the predictive model itself has the characteristic of solving the optimal solution, the proposed method can achieve stable suspension of the rotor. The proposed FD-SMPTC also has good dynamic performance and power generation stability.

ACKNOWLEDGEMENT

This project was sponsored in part by National Natural Science Foundation of China (62273168).

REFERENCES

- [1] Ooshima, M., A. Chiba, T. Fukao, and M. A. Rahman, "Design and analysis of permanent magnet-type bearingless motors," *IEEE Transactions on Industrial Electronics*, Vol. 43, No. 2, 292–299, 1996.
- [2] Asama, J., A. Mouri, T. Oiwa, and A. Chiba, "Suspension force investigation for consequent-pole and surface-mounted permanent magnet bearingless motors with concentrated winding," in *2015 IEEE International Electric Machines & Drives Conference (IEMDC)*, 780–785, Coeur d'Alene, ID, USA, 2015.
- [3] Diao, X., H. Zhu, Y. Qin, and Y. Hua, "Torque ripple minimization for bearingless synchronous reluctance motor," *IEEE Trans-*

- actions on Applied Superconductivity*, Vol. 28, No. 3, 1–5, Apr. 2018.
- [4] Ooshima, M., S. Kitazawa, A. Chiba, T. Fukao, and D. G. Dorrell, “Design and analyses of a coreless-stator-type bearingless motor/generator for clean energy generation and storage systems,” *IEEE Transactions on Magnetics*, Vol. 42, No. 10, 3461–3463, Oct. 2006.
- [5] Tomlinson, M., H. d. T. Mouton, R. Kennel, and P. Stolze, “A fixed switching frequency scheme for finite-control-set model predictive control — Concept and algorithm,” *IEEE Transactions on Industrial Electronics*, Vol. 63, No. 12, 7662–7670, 2016.
- [6] Cortes, P., S. Kouro, B. L. Rocca, R. Vargas, J. Rodriguez, J. I. Leon, S. Vazquez, and L. G. Franquelo, “Guidelines for weighting factors design in model predictive control of power converters and drives,” in *2009 IEEE International Conference on Industrial Technology*, 1–7, 2009.
- [7] Muddineni, V. P., A. K. Bonala, and S. R. Sandepudi, “Enhanced weighting factor selection for predictive torque control of induction motor drive based on VIKOR method,” *IET Electric Power Applications*, Vol. 10, No. 9, 877–888, 2016.
- [8] Muddineni, V. P., S. R. Sandepudi, and A. K. Bonala, “Finite control set predictive torque control for induction motor drive with simplified weighting factor selection using TOPSIS method,” *IET Electric Power Applications*, Vol. 11, No. 5, 749–760, 2017.
- [9] Davari, S. A., D. A. Khaburi, and R. Kennel, “An improved FCS–MPC algorithm for an induction motor with an imposed optimized weighting factor,” *IEEE Transactions on Power Electronics*, Vol. 27, No. 3, 1540–1551, Mar. 2012.
- [10] Justo, J. J., F. Mwasilu, E.-K. Kim, J. Kim, H. H. Choi, and J.-W. Jung, “Fuzzy model predictive direct torque control of IPMSMs for electric vehicle applications,” *IEEE/ASME Transactions on Mechatronics*, Vol. 22, No. 4, 1542–1553, Aug. 2017.
- [11] Dragičević, T. and M. Novak, “Weighting factor design in model predictive control of power electronic converters: An artificial neural network approach,” *IEEE Transactions on Industrial Electronics*, Vol. 66, No. 11, 8870–8880, Nov. 2019.
- [12] Rojas, C. A., J. Rodriguez, F. Villarroel, J. R. Espinoza, C. A. Silva, and M. Trincado, “Predictive torque and flux control without weighting factors,” *IEEE Transactions on Industrial Electronics*, Vol. 60, No. 2, 681–690, Feb. 2013.
- [13] Ravi Eswar, K. M., K. V. P. Kumar, and T. V. Kumar, “Modified predictive torque and flux control for open end winding induction motor drive based on ranking method,” *IET Electric Power Applications*, Vol. 12, No. 4, 463–473, 2018.
- [14] Norambuena, M., J. Rodriguez, Z. Zhang, F. Wang, C. Garcia, and R. Kennel, “A very simple strategy for high-quality performance of AC machines using model predictive control,” *IEEE Transactions on Power Electronics*, Vol. 34, No. 1, 794–800, Jan. 2019.
- [15] Zhang, Y., B. Zhang, H. Yang, M. Norambuena, and J. Rodriguez, “Generalized sequential model predictive control of IM drives with field-weakening ability,” *IEEE Transactions on Power Electronics*, Vol. 34, No. 9, 8944–8955, Sep. 2019.
- [16] Li, Y. and H. Zhu, “Three-vector model predictive suspension force control for bearingless permanent magnet slice motor,” *IEEE Transactions on Power Electronics*, Vol. 38, No. 7, 8282–8290, Jul. 2023.